Nanoscale

Accepted Manuscript

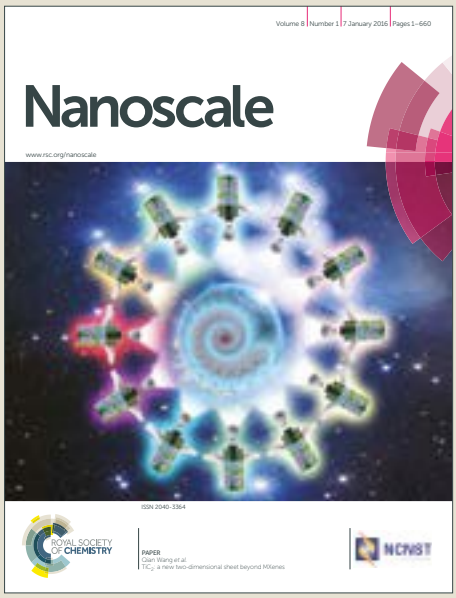

ROYAL SOCIETY OF CHEMISTRY

rsc.li/nanoscale

Journal Name

ROYAL SOCIETY OF CHEMISTRY View Article Online
DOI: 10.1039/C8NR09911A

ARTICLE

Gold nanoholes fabricated by colloidal lithography: novel insights in nanofabrication, short-range correlation and optical properties

RIReceived 00th January 20xx,
Accepted 00th January 20xx

DOI: 10.1039/x0xx00000x

www.rsc.org/

Maura Cesaria[a,b], Antonietta Taurino[a,*], Maria Grazia Manera[a], Maria Minunni[b], Simona Scarano[b], and Roberto Rella[a]

Colloidal lithography is widely used as a low cost and large-area deposition approach, alternative to the conventional small-area expensive lithographic techniques, for the fabrication of short-range ordered sub-wavelength metallic nanostructures.

This paper contributes to the understanding of the impact of the fabrication protocol of a colloidal mask on the optical and sensing properties of SR-ordered nanohole (NH) distributions fabricated by colloidal lithigraphy in optically thin (20 nm thick) gold films. We consider polystyrene nanospheres with nominal diameter of 80 nm, electrostatically adsorbed from a salt-free colloidal solution onto a polydiallyldimethylammonium (PDDA) countercharged monolayer. By avoiding the conventional polyelectrolyte multilayer and based on the interplay between the deposition times of both PDDA and PS-NSPs, we demonstrate effective simplification of the commonly applied deposition protocol and effective tuning of the NH-to-NH spacing (d_{NN}) with negligible agglomeration. Comparison with NH samples prepared by salt-containing colloidal solutions points out the negative impact of salt addition on the optical properties. The effective tuning of d_{NN} obtained by our protocol demonstrates high correlated disorder under unsaturated adsorption and lets discuss the analogies of the optical response between long- and short- range ordered NH systems, which is a still debated topic. By Fast Fourier Transform of autocorrelation image we demonstrate quantitatively, rather than in principle, the correspondence between an inherent ordering length-scale and d_{NN}. As optical transducers for detecting refractive index changes, our samples exhibit significant bulk sensitivity (~309 nm/RIU) in the framework of short range ordered NH systems.

1. Introduction

Spectral resonances, a small dispersion angle of the transmitted beam and transmission enhancement unpredicted by the Bethe's classical theory[1] have been reported in sub-wavelength holes periodically milled in an optically thick metal film[2,3]. These phenomena were first attributed to resonant excitation of Bloch-wave surface plasmon polaritons (SPPs) by a grating coupling mechanism to free-space photons at the metal-dielectric interface[4]. The matching-momentum condition implies discrete resonance wavelengths depending on lattice geometry and periodicity, choice of metal and dielectric environment, and incidence angle of the exciting light with respect to the normal to the metal-dielectric interface [5-7]. Two distinct and independent sets of transmission resonances are associated with the bottom and upper side of an optically thick (>100 nm) metal nanohole-slab sandwiched between dielectrics with different refractive index. Decreasing film thickness down to several units of the metal skin depth couples the transverse magnetic SPP modes from one side of the film to the other into the so-called long range SPP mode and short range SPP mode[8,9].

Unlike the original assumption that the transmission maxima of a nanohole (NH) array are associated with Bloch-wave SPPs[2], experimental evidences demonstrated transmission maxima red-shifted with respect to the theoretical prediction[5,7,10,11] as well as correlation between transmission minima and propagating SPPs in the case of optically thin films[2,6,12-14].

Concerning the mechanism of enhanced transmission in NH arrays, originally it was assumed that the enhanced fields associated to the propagating SPP modes excited on top and bottom interfaces reinforce the evanescent field within the NHs contributing to funnel the incident light through the metal film[15,16]. Alternative models included NH waveguide modes and interference between the SPP modes launched from the NHs[13,17] leading to account for localized surface plasmon resonance (LSPR) around individual NHs and propagating surface plasmon resonance (PSPR) along the metal surfaces. Therefore, in general optical spectra include contribution from LSPRs, PSPRs and Wood's anomalies[18]. The richness of plasmonic modes supported by NH arrays is particularly important because of potential applications in several fields [19-35]. Indeed, the peculiar electric field enhancement of the

[a] Institute for Microelectronics and Microsystems, IMM-CNR, Via Monteroni, I-73100 Lecce, Italy.
[b] Università degli Studi di Firenze, Department of Chemistry "Ugo Schiff", Via della Lastruccia 3-13, 50019, Sesto Fiorentino, Firenze (Italy)
*Email: antonietta.taurino@le.imm.cnr.it

DOI: 10.1039/C8NR09011A

plasmonic modes excited at the metal-dielectric interface can significantly influence surface-driven optical processes and be sensitively influenced by interface molecular binding-induced refractive index changes in real time biomolecular analysis [32].

The manufacturing of periodic arrays of nanometer scale metallic features with controllable size, shape, arrangement and coupling degree, demands specialized top-down nanofabrication techniques[32,34,36-47] which, however, are poorly cost effective, time-consuming, unsuitable for both patterning of areas larger than tens to hundreds of μm^2 and mass production of ordered NH arrays. Alternatively, some large-scale nano-patterning approaches have been proposed for less expensive high-throughput fabrication of NH arrays: among others, template stripping[48], soft interference lithography[49,50] and modified nanosphere lithography[51] where monolayers of close-packed hexagonal lattice self-assembled (silica, latex or polystyrene) nanospheres are used as deposition and/or etching masks and easily removed by tape stripping. The attractive features of this technique are low cost, high reproducibility, the formation of 10-100 μm^2 extended defect-free self-assembled domains, the ability to produce well-ordered (periodic) arrays and coupling with other methodologies[52]. Colloidal lithography has recently emerged as a very simple and versatile approach to fabricate short-range arrayed NHs based on colloidal masks with a reproducible distribution over a large area and without formation of neighboring domains with defective boundaries[53]. The working principle of colloidal lithography relies on adsorption, driven by electrostatic interactions, of likely-charged polymeric colloids onto a substrate preliminary modified by the deposition of a polyelectrolyte multilayer to carry out a surface charge opposite to the one of the adsorbing colloids. The practical convenience in fabricating short-range ordered NH arrays by means of colloidal lithography has raised the fundamental question of the excitation of delocalized SPR modes in absence of periodicity, as well as has focused interest on the NH-related LSPR modes and NHs acting as sources-and couplers of propagating SPR waves[13,17,54]. Studies on SR-ordered NH distributions at both fundamental and applicative level aim at gaining insight into the role and extent of ordering scale-lengths[13,45,55-58] and the mechanisms responsible for resonant transmission features even in absence of long-range order[13,14,59]. Several applicative opportunities resulting from the excitation of SPR modes have been reported, in particular as concerns refractive index changes monitoring at the metal-dielectric interface [30,60,61].

This paper aims at contributing to understand optical properties of short-range-ordered NH arrays as related to their distribution which might be tuned by means of a proper fabrication protocol of the colloidal mask. Optimization of the fabrication protocol was a fundamental concern of our studies for ensuring a proper tuning tool of NH array distribution and therefore of the related optical response.

In particular, we present and discuss NH systems fabricated by colloidal lithography in optically thin (20 nm thick) gold (Au) films as a function of the average NH-to-NH spacing, in the absence of electrostatic shielding between the polystyrene colloids and using a single polyelectrolyte binding layer. Unlike our protocol, in general, a polyelectrolyte multilayer with a surface charge opposite to the one of the colloids is deposited [53,59,62]. Based on the interplay of the deposition times of both polyelectrolyte monolayer and polystyrene nanospheres, we demonstrate that the commonly applied deposition protocol can be greatly simplified while providing tunable coverage and correlated disorder of the polystyrene nanospheres with minimal detrimental effects of agglomeration.

By comparison with NH arrays prepared by colloidal solutions containing intentionally added salt, our results point out the negative impact that salt addition may have on the optical properties of NH systems. Interplay between concentration and salt-content of the nanosphere solution, deposition time and heat treatment of the deposited mask were already investigated[59] with the aim of achieving control over the coverage of the colloidal mask but missing a proper discussion on the related morphological properties of the NH arrangements. On the contrary, our study comprehensively discusses and correlates structural and optical properties of short-range-ordered NH distributions.

Firstly, we explore the distribution characteristics of the colloidal mask and point out relevant ordering differences between salt-based and salt-free samples providing evidence that unshielded rather than shielded inter-colloid electrostatic repulsion yields short-range-ordered and well-separated NHs with controllable and tunable coverage. Moreover, the NH-to-NH spacing dependence of the optical response provides evidence of analogies between long- and short- range NH systems, which is a still debated topic.

Finally, we explored the applicability of the fabricated NH arrays as optical transducers by investigating the corresponding optical phenomena in the sensing field for monitoring plasmon resonance shifts upon refractive index changes at the metal interface. It was demonstrated that significant sensing performance can be achieved in the framework of the SR-ordered metallic NH structures.

2. Experimental details

2.1. Fabrication protocol

Microscope glass slides, thoroughly cleaned by ultrasonication in acetone (Sigma Aldrich) at 60°C for 20 minutes and isopropylic alcohol (Sigma Aldrich) at 60°C for 20 minutes followed by careful drying with N_2-stream, were used as substrates. They were processed with oxygen-plasma (100 sccm, 50 Watt, 250 mTorr, 1min process time) (Fig. 1(a)) to induce a negatively charged surface prior to be immersed in an aqueous solution of the positively charged polydiallyldimethylammonium (PDDA) (MW 200000–350000, Sigma Aldrich, 0.2 wt % in Milli-Q water) polyelectrolyte (Fig. 1(b)) for different dipping times (Δt_{PDDA}= 40 s, 1 min, 2 min).

The deposited PDDA layer was carefully rinsed with deionised water and blow-dried under N_2 flow. We deposited a single PDDA binding layer rather than the usually deposited multi-layered polyelectrolytes and the selected concentration of the salt-free PDDA solution guarantees unscreened strong intra-

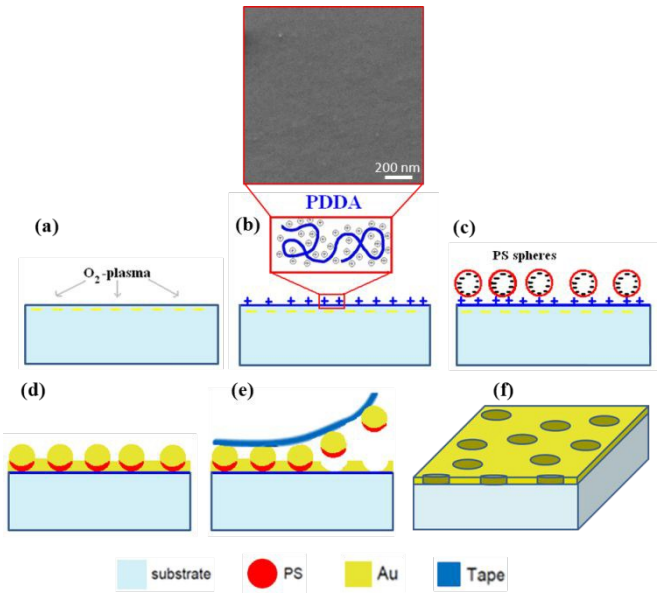

Figure 1. Sketch of the experimental protocol applied to fabricate Au NHs onto glass substrates by colloidal lithography. (a) Oxygen plasma treatment applied to the substrate to enable (b) binding by electrostatic attraction of a PDDA layer. (c) Adsorption of the likely charged PS-NSPs followed by (d) thermal evaporation of a Au film and (e) removal of the Au-capped PS-NSPs by tape stripping. (f) The resulting structure is an Au film perforated with circular sub-wavelength NHs.

chain and inter-chain electrostatic repulsion, leading to easier adsorption and flat configuration of the adsorbed chains with flatness enhanced by the attractive substrate[63,64]. Under these conditions, increased coverage of the PDDA layer is ruled by an increase of Δt_{PDDA} beyond 40 sec, accounting that the adsorption of PDDA monolayers was reported to reach 90% saturation in 40 sec[65].

The procedure applied for depositing the colloidal mask is sketched in Fig 1(c): the substrates covered by a PDDA layer were immersed, for a time Δt_{PS} ranging from 1 to 10 min, into a salt-free aqueous dispersion (0.1% wt) of commercial sulfate stabilized PS-NSPs (ThermoFisher Scientific) with nominal diameter D_{PS}= (80±4) nm.

The adsorption step of the colloidal mask was followed by rinsing off any excess of unbounded PS-NSPs with deionised water, immersion of the samples in distilled water at 100°C for 1 minute and careful N_2 blow-drying.

In order to fabricate metallic NH systems, the obtained distributions of PS-NSPs were covered by a thermally evaporated (20±2) nm thick gold (Au) film (Fig. 1(d)). Subsequent removal of the Au-capped colloidal mask by tape stripping (Fig. 1(e)) resulted in an optically thin (20 nm) Au film perforated with NHs onto a glass substrate (Fig. 1(f)). Based on the fabrication protocol (tape stripping removes the polystyrene beads and leaves NHs), colloidal masks and associated NH arrays have perfectly overlapping distributions. Definitively, diameter (D_{NH}) and arrangement of the NHs are controlled by the size (i.e., $D_{NH} \sim D_{PS}$) and arrangement of the PS colloidal mask.

Table 1. Colloidal masks deposited by colloidal lithography with the corresponding experimental details and results of the statistical analysis

Colloidal mask	Δt_{PDDA}	Δt_{PS}	C_{NaCl}	d_{NN} (nm)
PS_{NaCl}(40s-1min) NH_{NaCl}(40s-1min)	40 sec	1 min	2 mM	NA
PS(40s-5min)	40 sec	5 min	0 mM	161±32
PS(40s-10min)	40 sec	10 min	0 mM	156±32
NH_{NaCl}(1min-50s)	1min	50sec	2mM	105±20
PS(1min-50s) NH(1min-50s)	1min	50sec	0mM	192±31
PS_{NaCl}(1min-3min)	1 min	3 min	2 mM	92±22
PS(1min-3min)	1 min	3 min	0 mM	141±31
PS(2min,1min)	2 min	1 min	0 mM	110±22

About materials, Au is often the material of choice for the fabrication of NH arrays because it does not suffer from oxidation, is chemically unreactive and provides a very high optical resonance transmission[66].

Based on the experimental protocol, throughout the paper the fabricated distributions of Au-capped polystyrene nanospheres (Fig. 1 (d)) will be termed PS(Δt_{PDDA}-Δt_{PS}), where PS stands for "polystyrene", Δt_{PDDA} and Δt_{PS} refer to the duration of the deposition step of the PDDA layer and polystyrene colloids, respectively. Straightforwardly, the associated Au NH structure (Fig. 1(f)) will be termed NH(Δt_{PDDA}-Δt_{PS}), where NH stands for "nanohole distribution".

Aqueous suspensions of polystyrene beads containing NaCl salt (99.5% Sigma) with concentration C_{NaCl}=2mM were also prepared to allow nanospheres getting closer in the distribution. The colloidal/nanohole arrangements resulting from salt addition to the polystyrene suspensions will be termed PS_{NaCl}(Δt_{PDDA}-Δt_{PS}) and NH_{NaCl}(Δt_{PDDA}-Δt_{PS}), with the addition of the pedix "NaCl" to indicate the presence of NaCl in the starting colloidal solutions. For the reader guidance, Table 1 lists the experimental conditions for each sample (colloidal mask and NH array).

2.2. Morphological and optical analyses of the samples

The distributions of Au-capped polystyrene nanospheres deposited by colloidal lithography were investigated by scanning electron microscopy (SEM) and information about the arrangement of the associated NH samples was consequently derived.

A Zeiss NVISION 40 dual beam Focused Ion Beam (FIB) system, equipped with a high resolution SEM Gemini column and an Oxford 350 x-act Energy Dispersive X-ray Spectrometer (EDS), was used for the analysis.

SEM images were processed by using the Digital Micrograph software[67]. In particular, autocorrelation and Fast Fourier Transform (FFT) image processing tools, which are commonly used for the analysis of high resolution lattice images obtained by Transmission Electron Microscopy (TEM), were applied to SEM images, by virtue of their peculiar morphological features, i.e. presence of holes or spheres, which can locally give rise to periodic structures, like atoms in a crystalline lattice. FFT represents the image in the Fourier or frequency domain, where each point corresponds to a particular frequency contained in

the spatial domain image. Then, the presence of intensity maxima in the FFT is associated to spatial frequencies, i.e. to periodic structures of the image, like for lattice fringes in high resolution TEM images, whereas the absence of intensity maxima means absence of order, like in the case of amorphous materials. The autocorrelation image describes how well an image correlates with itself under conditions where the image is displaced with respect to itself in all possible directions; the result is a new image where periodic components are reinforced and noise is reduced. Then, FFT applied to autocorrelation images instead of to original images may allow a straightforward observation of the spatial frequencies corresponding to periodic structures which cannot be easily observed in the real image, due to their very short-range periodicity[68]. To our best knowledge, this kind of analysis were never applied for studying inherent ordering scales of short-range-ordered NH systems.

Turning to the optical characterization of the NH array structures, the zero-order transmission spectra were recorded by a Cary 500 UV-VIS-NIR Spectrometer (Varian, USA) in air by passing white light at normal incidence through the Au NH film supported onto a glass substrate. All spectra were acquired in the spectral range from 400 to 800 nm and normalized to the transmission of a bare glass substrate. Diffuse reflectance spectra (R) were also recorded at normal illumination in the range from 400 to 800 nm by the same Cary 5000 UV-VIS-NIR Spectrometer (Varian, USA) in its reflectance configuration equipped with an integrating sphere. Angle-dependent transmittance was measured in air by placing a linear polarizer between the incident beam and the sample and for incidence angle ranging from zero (normal incidence) to 50° by using a Cary500 UV-visible spectrophotometer integrated with a manually driven rotating stage. All spectra were acquired with a spectral resolution $\Delta\lambda$= 1 nm.

Sensing experiments were performed by simply immersing the sample under consideration in subsequent liquid environments with refractive index increasing from 1.33 (water) to 1.38 (mixtures of glycerol and water) and by detecting the shift of the wavelength position of the transmission maximum and minimum upon refractive index (RI) variation in a range of interest for biological applications. This procedure enabled to evaluate the bulk sensitivity $S_b = \Delta\lambda / \Delta RI$. The characterization of the plasmonic transducer in liquid phase was accomplished by a compact optical fiber system equipped with a deuterium halogen light source, a portable spectrometer (Thorlabs CCS100/M, wavelength ranging between 350÷700nm), and a system of optical fibers in transmission configuration. White light (450 to 700 nm) emerging from the first optical fiber entirely immersed into the liquid phase was perpendicularly shed onto the samples and the transmitted signal was coupled into a detection fiber and analyzed by using the compact UV–vis spectrometer.

3. Results and discussion

Unlike completely disordered NH distributions, quasi-periodic[69,70] and short range-ordered[13] NH arrays present transmission maxima and minima in the optical spectrum similar to the ones supported by periodic systems. This finding suggests that the presence of correlated disorder is in principle requested to observe transmission peaks and dips related to the coupling of the incident light with NHs acting as scatterers and sources of PSPR modes[13]. Turning from long-range to short range-ordered NH arrangements, changes in the average center to center distance of nearest neighbor NHs were assumed as the equivalent, at a first approximation, to changes of the periodicity parameter of the ordered-system counterpart[14,59]. Comparative studies between the resonance wavelengths of ordered and short range-ordered NH systems pointed out deviations enhanced with increasing area fraction of NH[14]. Measurements of the transmission maxima of short range-ordered NHs versus the NH-to-NH separation were observed to exhibit a not clearly linear trend able to confirming the linear theoretical relationship between the PSPR wavelength and the periodicity in ordered NH arrays[59]. Hence, analogies and deviations of the optical behavior between long- and short-range ordered NH systems are still not clearly understood at the fundamental level. Since NH-to-NH relative spacing depends on the electrostatic stabilization of the colloidal mask, changes of the NH-to-NH distance may be associated to rearrangements in the mask pattern too. In this picture, understanding how the optical response of SR-ordered NH systems evolves depending on the NH distribution (NH-to-NH spacing and degree of correlated ordering) is demanding, in order to transfer the knowledge available on ordered systems and gain insight in the applicative impact and differences due to the short-range-ordering.

In this section, we present and discuss the results of our colloidal lithography fabrication procedure applied to both salt-free and low ionic-strength suspensions of polystyrene beads to show how the peculiarities of the distribution (inter-particle distance (d_{NN}) and local correlation) play a role in affecting the optical response of NH systems. Although increasing the fractional coverage of a colloidal mask allows achieving electrostatically stabilized distribution, this does not assure an increase of correlated disorder due to the impact of the capillary forces on the relative positioning of particles closely spaced at a threshold distance. We discuss this point by tuning the length-scale of the interparticle electrostatic repulsion as well as the deposition times tracing a step forward with respect to the literature that commonly reports only colloidal masks fabricated under saturation adsorption conditions. In the present work we develop our discussion based on a series of samples selected to provide increasing NH fractional coverage (i.e., decreasing d_{NN}) and correlated disorder of the NH distribution.

3.1. Rationalization of the colloidal deposition parameters

As the main focus of the present study is the interpretation of the optical spectra of short range-ordered NH structures as a function of d_{NN}, we omit details about the systematic study of the deposition protocol of the colloidal mask that will be the subject of a future paper. However, before discussing the correlation between ordering properties and optical behavior of short-range ordered NHs, we rationalize our choice of the experimental parameters that influence d_{NN}, in particular colloidal size, concentration of the colloidal solutions and salt concentration. These parameters were properly investigated and also on the basis of the information available in the

literature, fixed at their optimized values, whereas the adsorption times of PDDA and polystyrene colloids, namely Δt_{PDDA} and Δt_{PS}, were varied in order to tune d_{NN} and the optical properties of the relevant NH distribution.

As far as the colloidal size is concerned, it is worth noticing that the protocol was found to be repeatable and applicable for different colloidal size, which is expected because the interparticle spacing of an electrostatically driven arrangement is dictated by the interparticle mutual repulsion, controlled by the size and salt content. Larger diameters associated with larger surface charge provided rescalable interparticle spacing with analogous characteristics of the distribution. For instance, SEM images shown in Fig. 2 compare the colloidal distribution deposited under the same adsorption conditions of PDDA and polystyrene colloids, namely Δt_{PDDA}= 40 sec and Δt_{PS}=1min, and different colloidal diameter, namely D_{PS}= 80 nm (Fig. 2(a)) and D_{PS}=100nm (Fig. 2(b)).

The interparticle spacing was found to be (203±31) nm and (299±37) nm, respectively, consistently with the expectation that larger surface charge implies longer range of the interparticle Coulomb repulsion. The similar characteristics of the distributions demonstrate that our protocol can be reliably applied for differently sized colloids. Therefore, for the fabrication of gold NHs, polystyrene beads with diameter D_{PS}= 80 nm, smaller than the ones used in the literature, were selected in order to reduce the electrostatic repulsion and the influence of capillary forces as well as for sensing optimization (as it will be discussed later).

In regard to the concentration of the polystyrene colloidal solution, in the present study we set the value of 0.1% wt as done in ref. 59, which is the comparative work for our experiments. This value (0.1% wt) turned out to be suitable to control ordering and avoid aggregation up to the saturated adsorption as well as to enable a finer control of the deposition time, and, as a consequence, of the coverage, versus the adsorption time. Values larger than 0.1% wt, up to doubled concentration, resulted to be less effective in controlling aggregation for long-time adsorption as well as were unpractical to fulfill the relationship $d_{NN} > 2D_{NH}$ (see the section on sensing in nanohole systems) over a wide range of values of d_{NN}. For instance, the comparison between the distributions in Fig 2(c) and in Fig 2(b), obtained for , corresponding to colloidal concentration of 0.2% wt and 0.1% wt respectively, demonstrates the increased tendency of the beads to aggregate even at a Δt_{PS} as short as 1 min.

On the other hand, values of the colloidal concentration smaller than 0.1% wt yielded lower adsorption rate and, as a consequence, prolonged adsorption time of the colloidal solution was needed to achieve a coverage comparable with the ones enabled by the control value of 0.1% wt. Basically, interplay between colloidal concentration and adsorption time rules the fractional coverage, the coverage being proportional to the colloidal concentration for short-time adsorption. Final adsorption coverage is expected to be independent on the colloidal volume fraction under achievement of irreversible adsorption.

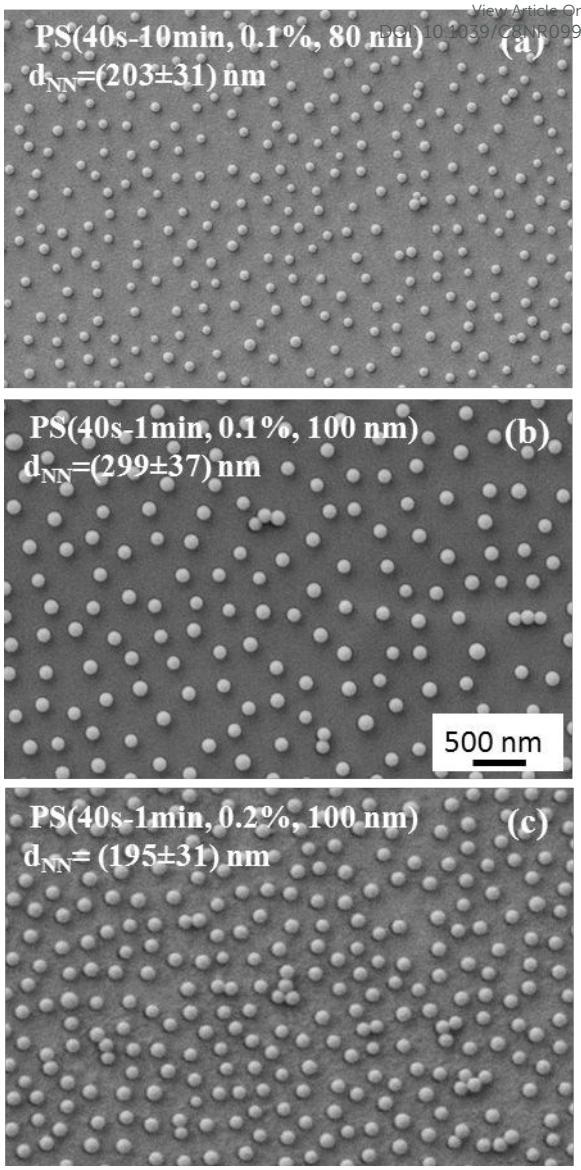

Figure 2. Plan-view SEM images of the polystyrene colloidal masks deposited by setting Δt_{PDDA}= 40 sec, Δt_{PS}= 1min and concentration of the colloidal solution at the value (a)-(b) 0.1 % wt and (c) 0.2% wt. The interparticle spacing evaluated by statistical analysis is also reported in each case.

Finally, concerning the impact of salt content on the NH distribution, C_{NaCl}=2 mM was set in the presented experiments as an upper value of ionic strength to illustrate and discuss the detrimental effects of salt addition on the NH distribution and optical response, as shown in the next paragraph. On the basis of our experimental findings, C_{NaCl} > 2 mM is not worth under our experimental conditions. On the other hand, decreasing C_{NaCl} with respect to 2 mM would correspond to increase the interparticle spacing, but effective control on the capillary-induced agglomerations, that in our experiments is favored by the decay-length of Coulomb repulsion between small sized colloids (D_{PS}= 80 nm), would be possible at just very low C_{NaCl}.

For instance, for C_{NaCl} progressively increased by doubling the salt concentration from zero to 2 mM (0, 0.5 mM, 1 mM, 2mM), the coverage of PS(1min-3min) distribution (see the discussion in the paragraph 3.2) was found to increase from 18.1% to 31.6% (18.1% at 0mM, 27% at 0.5 mM, 29% at 1 mM and 31.6% at 2mM), consistently with literature results[59], with agglomeration becoming more and more severe for increasing coverage. Notably, since the effect of capillary may overcome the Coulomb repulsion for interparticle spacing approaching the colloidal diameter, control on agglomeration would require, in principle, decay length of the Coulomb repulsion much larger than the colloidal diameter. Salt-related screening effects work against this issue and the more severely the smaller the colloidal diameter is. Furthermore, the presence of salt also favors disorder due to the screening of the colloid-PDDA substrate attraction.

In practice, for progressively increasing salt-content, the adsorption time requested to achieve the saturated adsorption gets shorter and shorter, leading to poor control of the range of achievable values of $d_{NN.}$.

More importantly, among the experimental parameters playing a role in tuning d_{NN} (i.e., colloidal diameter, concentration of the colloidal solution and range of the electrostatic repulsion), the presence of salt is the less controllable one in terms of ordering and capillarity effects.

Furthermore, the addition of salt could be not useful because decreasing d_{NN} below a values smaller than $2D_{NHI}$ is not desirable for sensing optimization of nanohole distributions (as it will be discussed later).

Definitively, to improve the repeatability of our protocol and limit the number of experimental parameters to be set, we used salt-free colloidal suspensions as a more practical and cheap condition, enabling more flexible tuning of the interparticle spacing by modulation only of the adsorption time (Δt_{PDDA} and, mainly, Δt_{PS}).

3.2. Ordering properties of the NH distributions

To our best knowledge using a polyelectrolyte monolayer rather than a multilayer in implementing colloidal lithography was not investigated in the literature properly. To date, a better colloidal mask was reported when using a triple polyelectrolyte layer rather than a PDDA monolayer for adsorption time of PDDA lasting 30 sec[71]. Also, colloidal masks were deposited onto a PDDA monolayer adsorbed for 30÷45 sec[72-73]. In order to assure an effective adsorption efficiency of colloids, in our experiments we considered Δt_{PDDA} ranging from 40 s to 2 min, that is at least the time needed to achieve 90% saturation adsorption[65].

As a preliminary check, we investigated the PDDA morphology by SEM analysis to ascertain the absence of surface features able to impact on the distribution of the overlying colloidal mask. For Δt_{PDDA} increasing from 40 sec to 5min, it was found in any case a very smooth surface, as suggested by the secondary electron image shown as an inset in Fig. 1(b), where no topographic contrast was observed in spite of the experimental conditions (50° sample tilt angle and accelerating voltage as low as 2kV) used to enhance this kind of contrast.

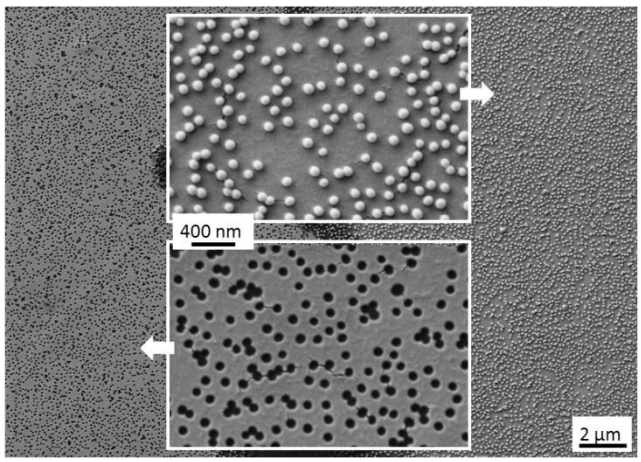

Figure 3. SEM images of Au-capped PS-NSPs (right-side panel and magnified uppermost inset) and corresponding NH distribution (left-side panel and magnified bottom inset) of the sample deposited under the experimental conditions Δt_{PDDA}= 40 sec, Δt_{PS} =1 min, and C_{NaCl}= 2 mM.

About the impact of Δt_{PDDA}, when Δt_{PDDA} increases from 40 sec (which would correspond to 90% saturation)[65] to 2 minutes, an increased binding efficiency can be achieved, in accordance with the literature[74].

Figure 3(a) shows SEM image of PS$_{NaCl}$(40s-1min) (right-side panel and magnified upper inset) and the corresponding NH distribution (NH$_{NaCl}$(40s-1min), left-side panel and magnified lower inset). The statistical analysis provided a NH diameter of nearly (81±7) nm, which is consistent with the nominal diameter of the polystyrene colloids.

The distribution of nanostructures (nanospheres and NHs) is quite inhomogeneous with large empty spaces in between and randomly formed agglomerates over the entire surface of the sample. Such features makes any estimation of an average inter-particle spacing meaningless from the point of view of short range-order. Hence, the deposition conditions (Δt_{PDDA}= 40 sec and Δt_{PS}= 1 min) are clearly unsuitable for fabricating NH structures with correlated disorder and NH-to-NH spacing close to the electrostatic equilibrium value. In order to improve uniformity and coverage of the distribution, Δt_{PDDA} was increased from 40 sec to 1 min while keeping Δt_{PS} as short as 50 sec to favor low coverage as a starting situation for calibration purposes of further experiments.

Figure 4(a) shows SEM plan-view image of NH$_{NaCl}$(1min-50s), briefly labeled by C_{NaCl}= 2mM in the transmission spectrum. As compared to NH$_{NaCl}$(40sec-1min), chain-like arrangements and more extended localized clusters of NHs (some examples are evidenced in the image by white rectangles and circles respectively) can be clearly observed resulting from improved NH coverage. The statistical analysis provided d_{NN}=(105±20) nm, corresponding to a surface fractional coverage of 25.3%.

By comparison, SEM plan view image of PS(1min-50s) in Fig. 4(b), that provides complete information about the distribution of NH(1min-50s), clearly demonstrates a reduction of agglomerates and more evenly distributed nanospheres

with d_{NN}=(192±31) nm. Interestingly, the comparison between the transmittance spectra of NH_{NaCl} (1min-50s) and NH(1min-50s) (briefly labeled by C_{NaCl}= 0mM) in Fig. 4(c) points out that the NH distribution is critical in determining the optical properties. Although both spectra exhibit a peak around 510 nm, the array obtained from salt-free solution presents a wide transmission band, which is almost featureless and flattened in the case of the salt-based sample. These results can be rationalized based on the shared evidence that the disorder causes decreased intensity and flattening (loss of structure) of the transmission spectrum of collective plasmonic modes supported by NH arrays [61].

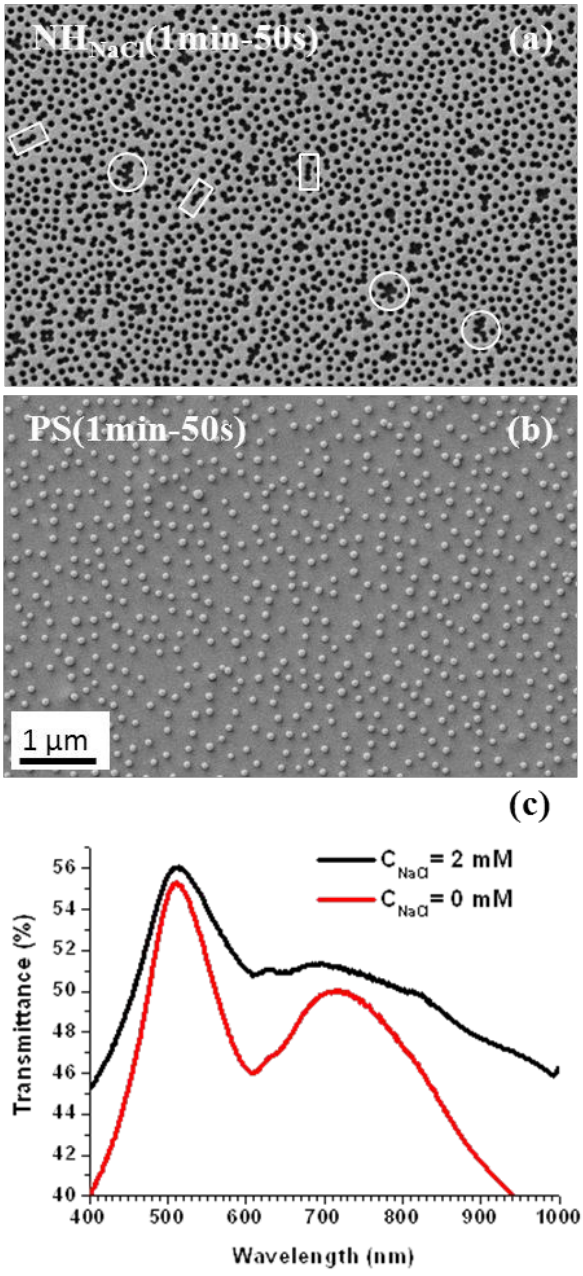

Figure 4. SEM image of (a) NH_{NaCl} (1min-50s) and (b) PS(1min-50s). (c) Zero-order normal incidence transmittance spectra of NH_{NaCl} (1min-50s) (black curve, C_{NaCl}=2mM) and NH(1min-50s) (red curve, C_{NaCl}=0mM).

This literature finding combined with the fact that quasi-periodic and short-range ordered NH distribution are needed to observe transmission resonances, confidently suggest that our results could be related to salt-induced reduced level of ordering. As a confirmation, the level of order of NH_{NaCl} (1min-50s) was investigated by autocorrelation and FFT analyses (images not reported here for the sake of brevity). This further investigation demonstrated total absence of ordering, which confirms that the flattening of the transmission band observed for C_{NaCl}= 2mM (Fig. 4(c)) is related to lack of ordering rather than high coverage. Hence, screened electrostatic repulsion between the polystyrene beads yields a reduction of the level of order under identical deposition conditions. On the other hand, C_{NaCl} = 0mM is expected to reduce the NH coverage, which is consistent with transmitted intensity lower for NH(1min-50s) than for NH_{NaCl}(1min-50s). About the persistent peak at 510 nm, it is worth noticing that it is narrower and blue-shifted with respect to the transmission maximum of the reference 20 nm thick Au film (located at 532 nm). Therefore it could be ascribed to the interplay between interband *sp-d* transitions of Au and plasmonic modes of the NH structure[42]. Based on angle-dependent measurements of the transmission spectrum of NH(50s-1min), the peak occurring at 700 nm was assigned to a LSPR mode.

In order to confirm the effects of the presence and absence of salt on tuning d_{NN} and degree of correlation, we prolonged Δt_{PS} from 50 sec to 3 min. In this respect, Fig. 5 (a) shows SEM plan-view image of PS_{NaCl}(1min-3min) to be compared with the analogue salt-free sample reported in Fig. 6(a). It is clearly observable that in the presence of salt the polystyrene nanosphere distribution is strongly inhomogeneous and dominated by the formation of void areas and severe agglomerates. The statistical analysis of PS_{NaCl}(1min-3min) provided d_{NN}=(93±22) nm and coverage c=31.6 %. On the contrary, the salt-free sample exhibits a uniform coverage corresponding to c=18.1% (i.e., d_{NN}=(141±31) nm) with quite negligible presence of void areas and agglomeration (Fig. 6(a)). Hence, under identical Δt_{PDDA} and Δt_{PS} deposition times, clustering of the polystyrene nanospheres can be more effectively controlled and avoided using colloidal salt-free aqueous solutions. These results are expected and can be accounted on the basis of the working principle of colloidal lithography. Indeed, self-assembly driven by the inter-colloid electrostatic repulsion results in different degree of short range ordering as well as coverage increasing upon increasing the adsorption time Δt_{PS} up to achieving the adsorption saturation. Although salt-induced screening effects would favor shortened nearest neighbor spacing, capillary forces can act as the inter-particle spacing is reduced below a threshold during drying[75,76]. All of this may result in either sparsely distributed polystyrene beads with large void areas in between (under low coverage situation) or highly aggregated polystyrene nanosphere distributions (under high coverage situation) with uncontrolled relative spacing and absence of a characteristic inter-particle distance representing a "real" average description of the nanosphere assembly and indicative of the short-range-ordering degree.

View Article Online
DOI: 10.1039/C8NR09911A

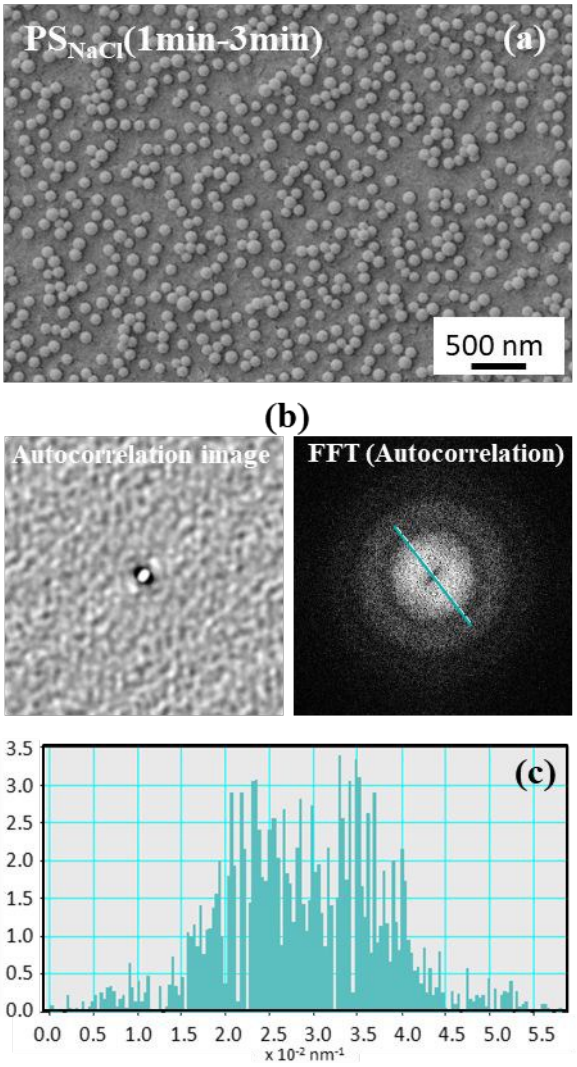

Figure 5. (a) Plan-view SEM image of PS$_{NaCl}$(1min-3min). (b) Distribution of the autocorrelation function and corresponding FFT pattern, referred to as FFT (autocorrelation), of PS$_{NaCl}$(1min-3min). (c) Intensity distribution of the FFT (autocorrelation) showing the absence of a periodicity length.

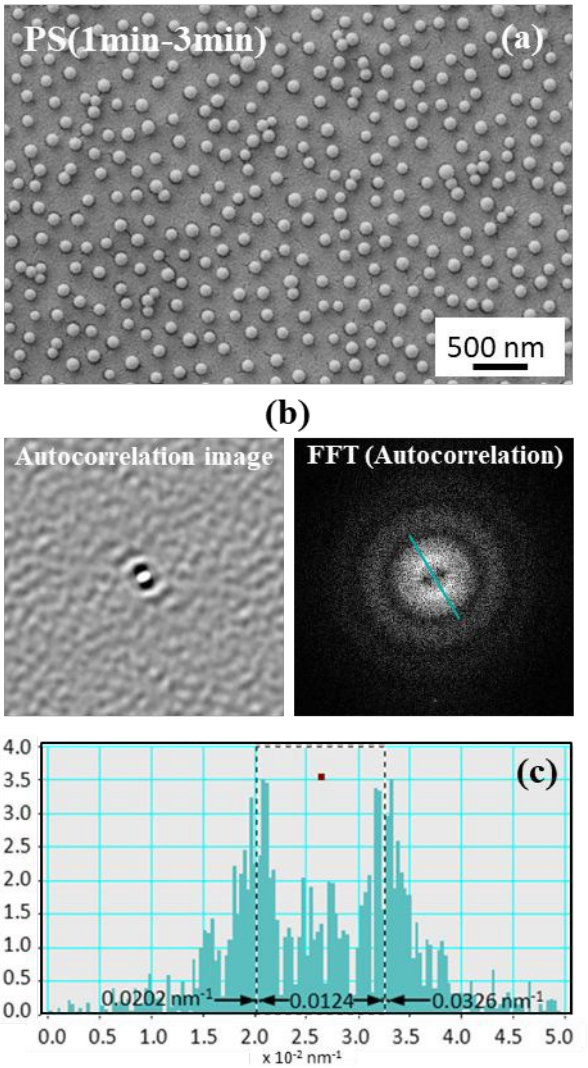

Figure 6. (a) Plan-view SEM image of PS(1min-3min). (b) Distribution of the autocorrelation function and corresponding FFT pattern (referred to as FFT (autocorrelation)), of PS(1min-3min). (c) Intensity distribution of FFT(autocorrelation) showing an intensity maximum corresponding to a periodicity length of 165 nm.

View Article Online
DOI: 10.1039/C8NR09011A

An estimation of the degree of correlated disorder in both PS_{NaCl}(1min-3min) and PS(1min-3min) was obtained by autocorrelation and FFT analysis of relevant SEM images[68], as shown in Figs 5(b) and 6(b), respectively. The autocorrelation function is not particularly informative: it presents a bright peak of correlation in the middle (corresponding to no shift of the image) and a background without evident periodicities indicating short range-ordering of the distribution. Nevertheless by comparing the FFT of the autocorrelation images of PS_{NaCl}(1min-3min) and PS(1min-3min), it can be noted that only in the case of the salt-free sample an intensity maximum, represented by two small arcs symmetrically placed around the center and corresponding to a spatial frequency of about 165 nm can be observed. This is demonstrated by the intensity line profiles of the FTTs reported in Figs. 5(c) and 6(c), obtained by sampling the FFT intensity along a line passing from the center and crossing the intensity maxima. Hence, in the presence of salt no ordering was ascertained. It is worth noticing that the estimated periodicity value of 165 nm is consistent with the statistical estimation d_{NN}=(141±31) nm, which demonstrates quantitatively and in practice, rather than in principle, a correspondence between the inherent ordering length-scale of a short-range-ordered NH distribution and the associated NH-to-NH spacing parameter d_{NN}.

Further experiments (not shown here) confirmed that, given Δt_{PDDA}=1 min and C_{NaCl}= 2mM, although Δt_{PS} prolonged up to 12 min induces the expected increased fractional coverage, the associated polystyrene nanosphere arrangements are characterized by dominance of randomly distributed severe agglomerates with voids in between.

Therefore, although in general increasing the coverage to achieve the electrostatically stabilized distribution is the key factor for improving the degree of correlated ordering of a colloidal mask, prolonging Δt_{PS} in the presence of electrostatic bead-to-bead shielding does not enable to effectively increase the coverage without capillary-induced detrimental effects of agglomerations.

By comparison with literature reports, a computational modeling of the colloidal adsorption processes indicated reduced correlated ordering under salt-addition[74]. The simulated colloidal distributions are unrealistic in that they present no agglomeration effects because the model, while including particle-particle interactions, particle-collector surface interaction and Brownian forces, rules out capillary lateral interactions. Unlike the computational model, our experimental distributions are affected from the capillary forces acting more effectively in the presence of salt and for increased coverage. Hence, our study demonstrates the practical impact of salt-addition on the colloidal distribution while tuning the interparticle distance.

Definitively, based on the remarks discussed in the paragraph 3.1 and the above experimental findings, under our experimental conditions, shielded electrostatic repulsion between polystyrene colloids demonstrated to be a not favorable strategy to fabricate short-range-ordered well-separated NHs with controllable average relative spacing.

To this aim, we adopted a different approach based on: i) salt-free solutions of polystyrene beads to be electrostatically assembled onto a PDDA single layer (Fig. 1(a)-(c)), ii) polystyrene nanospheres smaller than the ones usually reported in the literature to reduce the electrostatic repulsion and the influence of capillary forces, and iii) interplay between the deposition times Δt_{PDDA} and Δt_{PS}. For Δt_{PDDA}= 40 sec, we performed several experiments (not reported here) to get the value of Δt_{PS} providing D_{NH}/d_{NN} = 0.5 based on the reported result that the sensitivity of a NH structure increases linearly with the NH diameter-to-periodicity ratio and is enhanced around 0.5[75]. Under the condition Δt_{PS}= 5 min (sample PS(40s-5min), SEM image in Fig 7(a)), d_{NN}= (161±32) nm was obtained, corresponding to a coverage c=13.7 %. Increasing Δt_{PS} from 5 to 10 minutes (sample PS(40s-10min), SEM image in Fig 7(b)) resulted in d_{NN}= (156±32) nm, corresponding to c=15.3%.

Comparison between SEM images of PS(40s-5min) and PS(40s-10min) demonstrates similar distributions (meaning saturated adsorption around Δt_{PS}=5 min) with well-isolated nanospheres, no void areas and rare formation of small agglomerates. On increasing Δt_{PDDA} from 40 sec to 1 min, higher coverage was achieved upon increasing Δt_{PS} even at Δt_{PS} values shorter than 5 min, as SEM plan-view images of PS(1min-2min) (Fig 7(c)) and PS(1min-3min) (Fig 7(d)) clearly show. Statistical analysis provided the values d_{NN}=(178±30) nm (i.e., c=10.6%) for PS(1min-2min) and d_{NN}=(141±31) nm (i.e., c=18.1%) for PS(1min-3min), corresponding to a D_{NH}/d_{NN} ratio (where D_{NH} = 80nm) equal to 0.45 and 0.57, respectively. At least, PS(2min-1min) (Fig 7(e)) was found to exhibit the highest fractional coverage of PS beads (c=25.6%, d_{NN}=(110±22) nm) and sparsely distributed clusters. In any case correlated disorder can be observed with evident improved degree of local ordering with respect to the distributions resulting from intentional addition of NaCl salt. Notably, a linear relationship (R^2=99.9%) between the fractional coverage and d_{NN} was observed (Fig. 7(f)), reflecting the reproducibility of the series and the fact that d_{NN} represents a characteristic ordering distance determined by the deposition mechanism.

The evidence that prolonged Δt_{PDDA} enables to achieve higher coverage at shorter Δt_{PS} can be rationalized as follows.

While keeping Δt_{PS}=1 min, the slight increase in the surface coverage provided by increasing Δt_{PDDA} from 40 sec to 1 min suggests adsorption mainly ruled by the PDDA-polystyrene bead attraction through the improved surface coverage of the PDDA layer. Instead, while keeping Δt_{PDDA}=40 sec, the remarkable increase in the coverage resulting from an increase of Δt_{PS} indicates distribution dominated by the interparticle repulsion with no effective coverage improvement for Δt_{PS} prolonged beyond the saturated adsorption. In fact, the final distribution of the colloidal mask is dictated by the competition between the Coulomb attraction, that binds the colloids to the countercharged substrate, and the electrostatic repulsion between adsorbed and adsorbing likely-charged colloids.

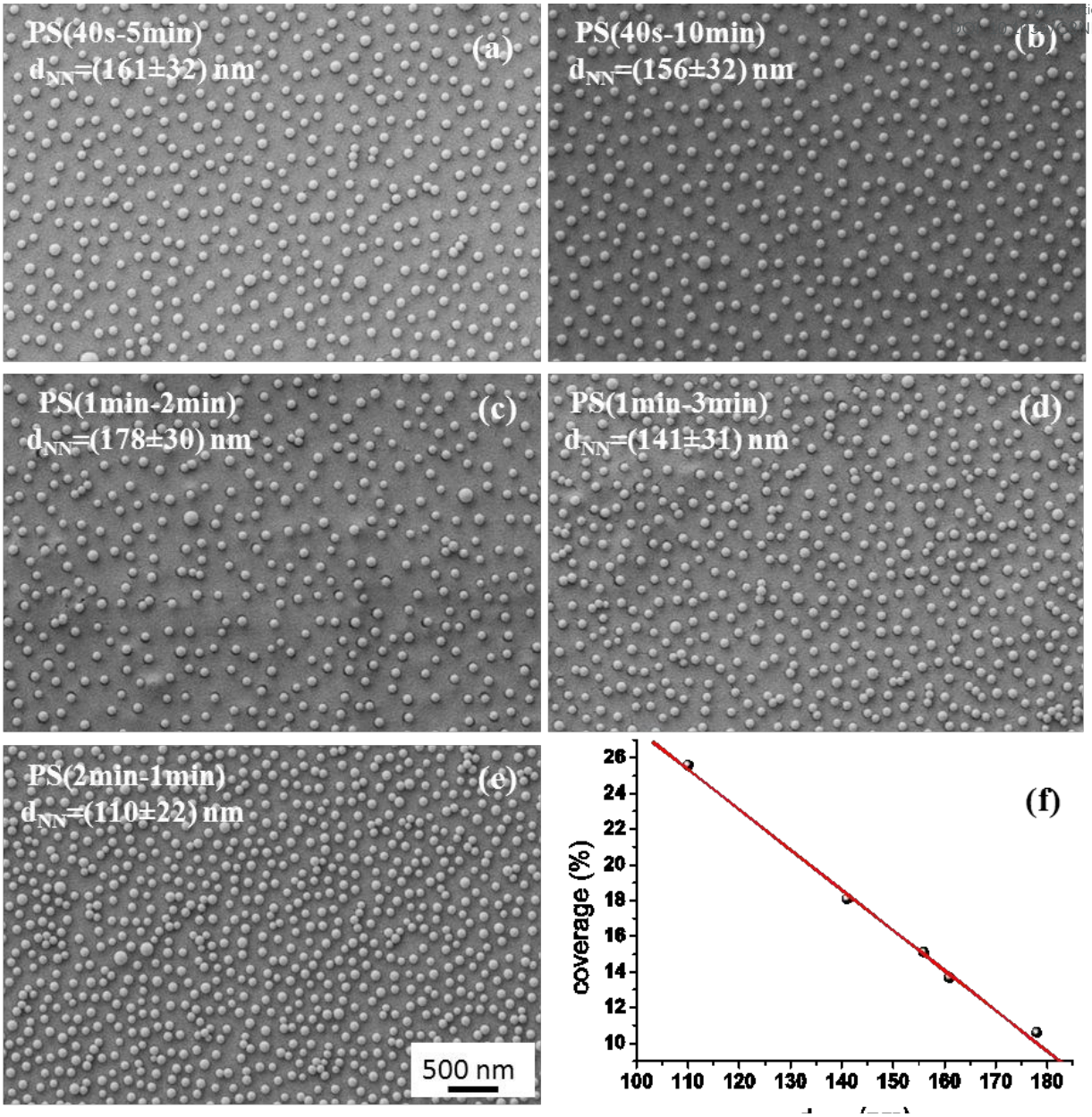

Figure 7. SEM images of the Au-capped PS-NSP distributions deposited for Δt_{PDDA}= 40 sec ((a) PS(40s-5min) and (b) PS(40s-10min)), Δt_{PDDA}= 1 min ((c) PS(1min-2min) and (d) PS(1min-3min)) and (d) Δt_{PDDA}= 2 min (PS(2min-1min)). The NH-to-NH average spacing d_{NN} resulting from the statistical analysis is also reported.

Hence, while the adsorbing nanospheres initially bind to the PDDA charged sites sparsely and randomly mainly depending on the zeta potential of the polyelectrolyte surface[71], for prolonged Δt_{PS} the arrangement is dominated by the electrostatic repulsion between the likely-charged polystyrene nanospheres below the threshold leading to severe clustering effects. Therefore, for salt-free colloidal solutions, the parameters playing a key role in the organization of the colloidal mask are Δt_{PDDA} and Δt_{PS}: Δt_{PDDA} affects charge distribution/coverage of the PDDA layer and Δt_{PS} rules the fractional coverage and ordering of the colloidal mask.

By comparison, the deposition conditions to achieve control on the coverage of a colloidal mask deposited onto a polyelectrolyte multilayer were explored in the literature based on the interplay between concentration (up to 0.12 % wt) and salt-content (up to 10 mM) of the colloidal solution as well as deposition time (from 30 s to 30 min) of the mask[59]. But the distribution/clustering characteristics of the colloidal mask and any correlated disorder difference between salt-based and salt-free samples were not investigated at all. About the obtained coverage, it was reported: i) surface coverage below 20% from salt-free colloidal suspensions by increasing the solution concentration up to 0.12 wt % and the deposition

time from 30s to 5 min, and ii) dense packing of the nanospheres (up to maximum coverage of 35%) with a 0.1 % particle concentration, salt content increased up to 10 mM and a deposition time of the mask prolonged up to 30 min. In general, achieving coverage higher than the needed one is useless for applications involving NH structures as it would introduce undesirable clustering effects with detrimental impact on ordering and optical properties. The NH fractional coverage should be kept within a certain range of the NH diameter-to-periodicity ratio to improve sensitivity, and control losses of the PSPR modes[77,78]. As a result of our experiments, we found surface coverage ranging from 10.6% (sample PS(1min-2min)) to c=31.6% (sample PS_{NaCl}(1min-3min)) by means of a simpler protocol based on the interplay between only two experimental parameters (Δt_{PDDA} and Δt_{PS}) and involving a single layer polyelectrolyte, short deposition times and no changes of the colloid concentration. Furthermore, our exploration of the configuration characteristics of the colloidal mask (well-separated as well as clustered particles) shows clearly that unshielded rather than shielded electrostatic repulsion between polystyrene colloids can yield short range-ordered well-separated NHs with controllable and tunable coverage even at relatively closely spaced NHs (sample PS(2min-1min) with coverage of 25.6%).
Definitively, our results demonstrate an actual simplification of the commonly applied layer-by-layer deposition and an effective ability to tune colloidal self-assembly with ordering performances comparable to literature reports using polyelectrolyte multilayers[62,71]. Unlike preparing polyelectrolyte multilayers, that demands preliminary polyelectrolyte-dependent study of the conditions for stable reconfiguration of the polymer chains and charge overcompensation[79,80], saturated adsorption and controlled morphology of a polyelectrolyte monolayer can be obtained very easily. Hence, our protocol represents a valid, easy and lower cost alternative to the conventional one.

3.3. Optical characterization

Once the distribution properties of the deposited samples were characterized thoroughly, their transmission spectra were inspected to ascertain the occurrence of the peculiar features of NH array. Our discussion will develop according to the following guidelines: i) checking changes in the transmission spectrum with the angle of incidence of the exciting light to assign experimentally the transmission features to either LSPR modes (which are unaffected by the incidence angle) or PSPR modes (which spectrally shift based on the momentum matching condition) [2,78,79], and ii) a comprehensive comparison with the literature of the optical behavior of our samples as a signature of the validity of the applied colloidal lithography protocol for fabricating NH distributions with correlated disorder.
Figure 8(a) shows the zero-order normal incidence transmittance (T) and reflectance (R) spectra as well as the calculated absorbance (Abs=100-R-T) of NH(40s-10min) chosen as a representative sample.

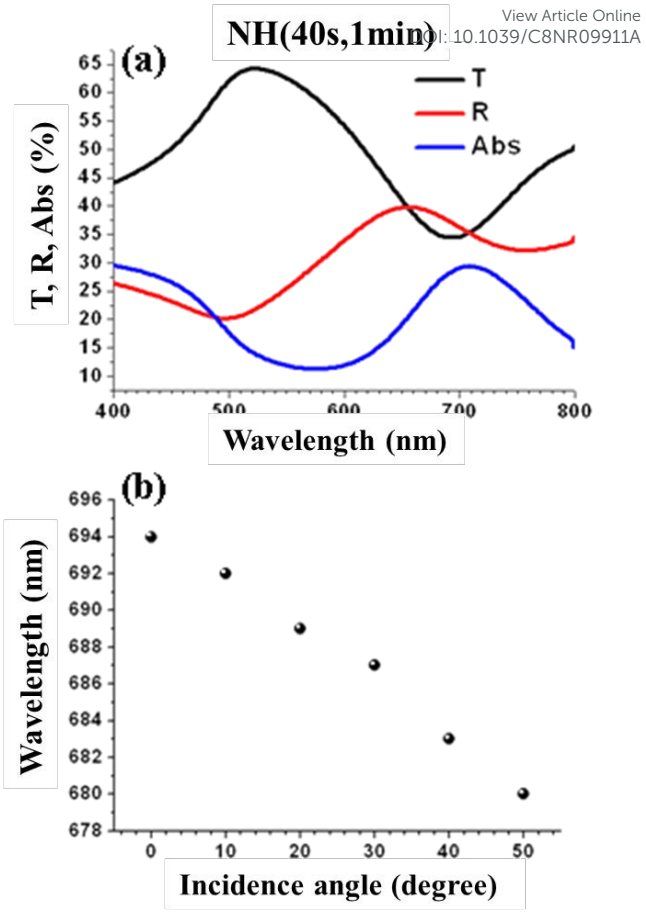

Figure 8. Optical characterization of NH(40s-10min) showing (a) normal incidence transmittance (T) and reflectance (R) spectra as well as the calculated absorbance (Abs=100-R-T), and (b) dependence of the wavelength position of the transmittance minimum on the incident angle.

Such un-polarized spectra are suitable to look for the spectral occurrence and position of the resonances, without loosing information, due to the short-range ordering of our samples and circular NH shapes that do not cause symmetry breaking[59]. Complementary reflectance and transmittance spectral features can be observed at slightly different wavelengths. In detail, transmission peaks (at 524 and 800 nm) and dip (at 693 nm) are associated with reflectance dips (a 496 and 770 nm) and peak (at 656 nm), respectively. This behavior was reported in short range-ordered NHs perforated in optically thin metal films as ascribed to interference between the directly transmitted/reflected light and the light first coupled into a propagating SPP mode and then coupled back to the initial direction of propagation[82,83]. Moreover, transmission maximum and minimum also correspond to absorbance minimum and maximum, respectively.
In order to correctly interpret the optical response of NH(40s-10min) arrays, some aspects have to be accounted for: i) the coupling between the long range-SPP and short range-SPP modes in optically thin films, ii) NH structures with asymmetric geometry (i.e., different uppermost and bottom dielectrics)

View Article Online
DOI: 10.1039/C8NR00911A

and thickness below 50 nm can support only the strongly damped short range-SPP mode as associated with a transmission minimum[84-86], iii) the resonant excitation of the short range-SPP mode in optically thin films can result in enhanced Abs and high R[83], iv) the absorbance maxima are linked to the transmittance minima due to enhanced absorption resulting from enhanced fields[88]. All of this would suggest that the transmittance minimum of NH(40s-10min) spectrally located at 693 nm could be associated with a PSPR mode. As a confirmation, the increase of light incidence angle from zero (normal incidence) to 50° results in a negligible shift of the transmission maximum at 524 nm and a blue-shift of the transmission minimum at 693 nm (Fig. 8(b))[78]. Therefore, the transmittance maximum at 524 nm and minimum at 693 nm correspond to PSPP and LSPP modes, respectively.

This attribution of a propagating-nature to the transmission minimum is consistent with the measured absence of spectral shift of the transmission minimum under changes of the incidence angle of *p*-polarized and *s*-polarized light, respectively[59].

In Fig. 9(a), the zero-order transmission spectra of NH(2min-1min), NH(1min-3min), NH(40s-10min), NH(40s-5min) and NH(1min-2min) (briefly named NH(2-1), NH(1-3), NH(40-10), NH(40-5) and NH(1-2) arrays, respectively) are compared as corresponding to d_{NN} increasing from 110 to 178 nm. Similar transmission features as the previously discussed sample (i.e., NH(40s-10min)) are shown. Hence, the assignment of the transmittance maximum and minimum to a LSPR and PSPR mode, respectively, can be confirmed for all the NH samples under study.

Moreover, the spectral positions of the transmittance maximum and minimum are consistent with the literature[85,87]. It can be observed that no loss of spectral features associated with either LSPR or PSPR occurs over the obtained coverage range (from 10 to 25.6%). This fact can be ascribed to d_{NN} values larger than $2D_{NH}$ (i.e., NH pattern with sufficient thin film surface to support PSPR and LSPR modes)[80] and electrostatically stabilized correlated disorder unaffected by capillary forces. As the spectral position of the transmission maximum is close to the one of the interband *sp-d* transitions of Au, the zero-order normal incidence transmission spectra of the NH structures were compared with the corresponding transmission through a 20 nm thick Au film (grey curve in Fig. 9(a)).

It can be observed that the transmittance peaks of the NH samples depend on the NH distribution, the corresponding bands are narrower than the Au band centered at 532 nm and their spectral positions don't match this wavelength value. As the transition peak of a Au film cannot depend on the presence of NHs, the transmission maximum of the NH arrayed film can be ascribed to the interplay between the interband *sp-d* transitions of Au and LSPR-related plasmonic modes supported by the NH structure[42,88]. Furthermore, the intensity of the transmission maximum does not increase on increasing number of NHs (i.e. on decreasing d_{NN}) and is lower than the transmission efficiency of the reference Au film. In

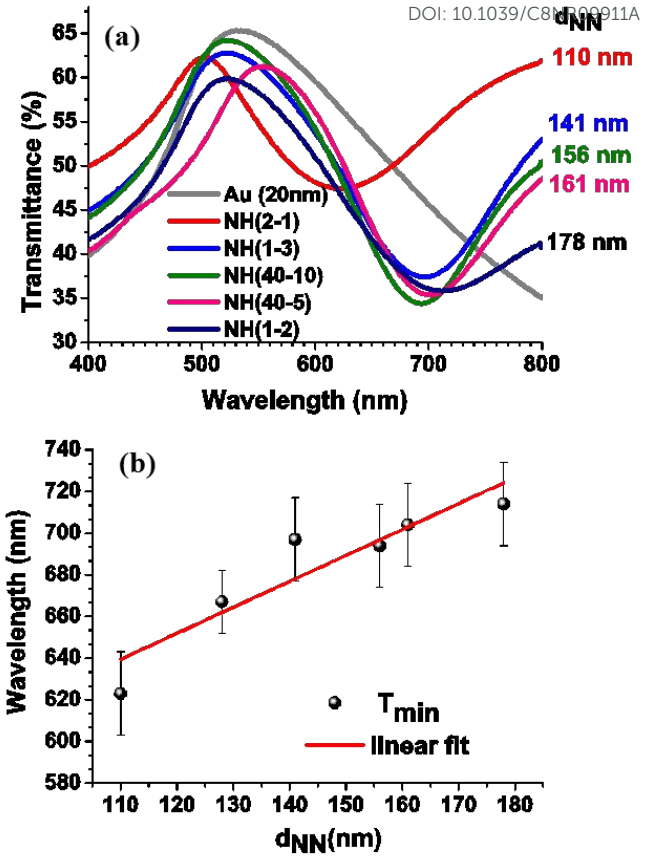

general, because of the absence of long-range order of the scatterers

Figure 9. (a) Zero-order transmittance spectra of the NH samples corresponding to d_{NN} increasing from 110 to 178 nm. (b) Dependence of the spectral position of the transmittance maximum on the NH-to-NH average spacing to d_{NN}.

(i.e., NHs), decreased transmission efficiency can arises from the interplay between multiple scattering from the SR-ordered NHs and material losses.

Our results are consistent with suppressed transmission reported for NH arrays fabricated in ultrathin (i.e., with thickness smaller or comparable to the skin depth) semitransparent films[85,89,90] and Au skin depth amounting to 20-35 nm[89]. Moreover, for d_{NN}=110 nm (i.e., NH(2min-1min)) the LSPR–related transmittance maximum blue-shifts, which can result from coupling between the localized modes of the neighboring NHs on increasing NH coverage[54].

Once our measurements of angle-dependent transmission let the attribution of the maximum and minimum to a LSPR and PSPR mode, respectively, an insight in the occurrence of analogies between ordered and short-range ordered NH systems can be investigated by the occurrence of an eventual relationship between d_{NN} and the wavelength of the PSPR mode. According to the grating-coupling condition, NH-to-NH spacing of a short range-ordered NH distribution corresponding to the lattice constant of a periodic NH array counterpart would imply a linear blue-shift in the PSPR

transmission feature. As the largest d_{NN} yielded by our NH samples is 178 nm, first order grating coupling wavelengths would be expected to occur below the lower limit set for the optical characterization (i.e., 400 nm). Dependence of the transmittance spectrum on the NH-to-NH spacing was reported in NH arrays non-diffractive in the visible range[59,87].

About the transmittance minimum (associated with a short range-SPP mode), Fig. 9(b) clearly shows that its spectral position increases almost linearly (R^2=83%) on increasing d_{NN} over the sampled range (from 110 to 178 nm). The experimental data associated with d_{NN}~141nm (NH(1min-3min)) and d_{NN}~110 nm (NH(2min-1min)) exhibit a slight deviation from the linear trend as compared to the other data. This effect could be ascribed to the presence of agglomerates in the distributions (SEM images in Figs 7 (d),(e)) that perturb the short-range ordering of the NH arrangements. Otherwise, the distribution of the experimental data in Fig. 9(b) could suggest the occurrence of two linear trends over contiguous ranges of values of d_{NN}. This point deserves deeper investigation, which is the subject of studies in progress.

Anyway, the clearly linear distribution of the spectral position of the transmittance minimum versus d_{NN} would suggest a few main conceptual remarks. First, keeping in mind the theoretical linear relationship between periodicity and wavelength of the PSPRs excited in periodic NH arrays, analogies between the optical behavior of PSPR modes in long- and short-range ordered NHs would be confirmed by our findings. Second, this observation is supported by the FFT analysis of the autocorrelation images that enables to disclose and measure very short-range periodicity and to correlate it with the NH-to-NH spacing calculated by the statistical analysis of SEM images which doesn't reflect periodic arrangements. Notably, this correspondence was found to hold for all the samples discussed in this study. At least, from the applicative standpoint, the above findings would demonstrate the occurrence of short range-ordering even under unsaturated adsorption of the colloidal mask resulting successfully from our simplified experimental protocol.

As a final comment, the same correspondence (i.e., complementary reflectance and transmittance features) noticed in then case of NH(40min-10min) was found for all the NH samples investigated in this study (Fig. 10). Also, the maximum absorbance is spectrally closed to the transmittance minimum (Fig. 10). All of this confirms the validity of our discussion on NH(40s-10min) as a representative sample and reliably enables us to extend the general discussion developed for NH(40s-10min) to all the other NH arrays presented in this study.

3.4. Refractometric sensing

Plasmonic nanohole arrays usually find application as refractometric sensors, exploiting their ability to detect refractive index changes at the metal/dielectric interface. The functional properties of a selected short range-NH array configuration have been investigated in this work. This choice is due to the following evidences: i) more homogeneous and

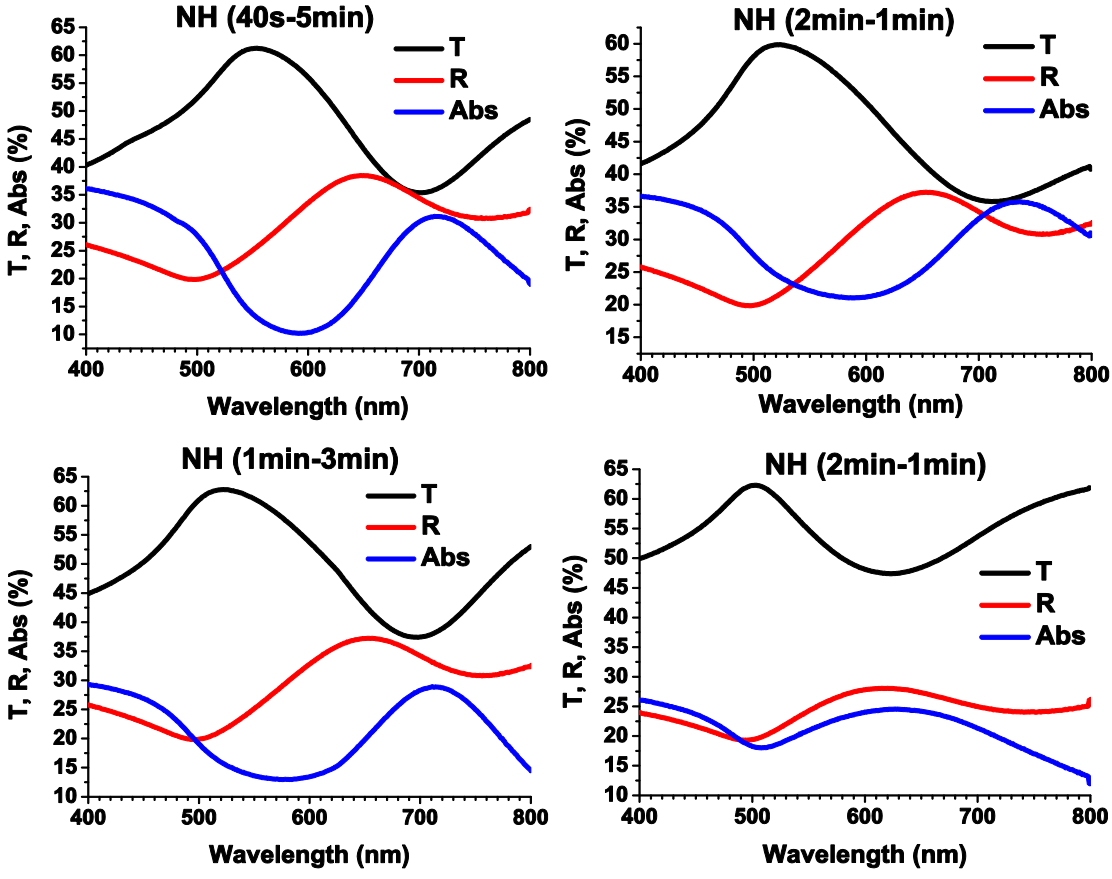

Figure 10. Zero-order transmittance (T), reflectance (R) and calculated absorbance (Abs) spectra of NH(40s-5min), NH(1min-2min), NH(1min-3min) and NH(2min-1min).

View Article Online
DOI: 10.1039/C8NR09911A

strong field enhancement inside the NH region was reported for SR-ordered NHs with diameter of 70 nm[92], and ii) the sensitivity increases linearly with the NH diameter-to-periodicity ratio and can be enhanced around the value 0.5 [68].

For this reasons, NH array resulting from NH(40s-10min) preparation conditions, (resulting in the following structural parameters: D_{NH}=80 nm, D_{NH}/d_{NN}=0.5) have been investigated as refractive index optical trasnducers. We have accounted for both the transmittance maximum (with localized character resonance, LSPR) and minimum (with propagating resonance character, PSPR).

A linear relationship between the shift of the transmittance maximum (Fig. 11(a)) and minimum (Fig. 11(b)) and the refractive index of the medium surrounding the sample NH(40s-10min) is evidenced. A red-shift of both the transmission peak and dip was measured on increasing refractive index that is more enhanced for the transmission minimum than for the transmission maximum wavelengths.

From a linear fit, the bulk sensitivity is determined: the value associated to the transmittance minimum and maximum was found to be (309±43) nm/RIU (R^2=98.7 %) and (38±10) nm/RIU (R^2=98.3%), respectively. This experimental finding is consistent with the propagating and localized character assigned

Figure 11. Plots showing the linear dependence on the

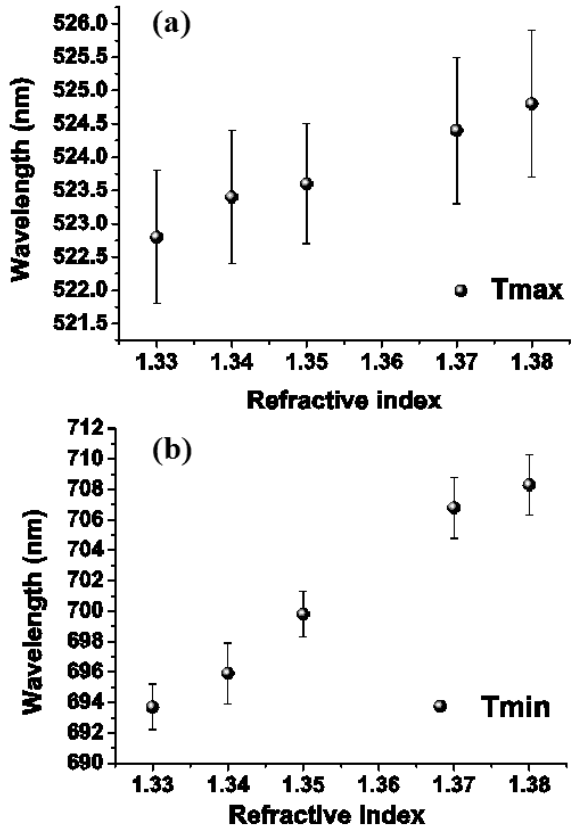

refractive index of the wavelength position of transmittance (a) maximum and (b) minimum of NH(40s-10min).

assigned to the transmittance dip and peak, respectively. Indeed, PSPRs and LSPRs are known to be more sensitive to bulk refracting index changes and molecular binding processes, respectively.

On the other hand, the measured value (309±43) nm/RIU is comparable with or even better than other reports[14,29,43,52,93-97]. In general, the bulk sensitivities from arrays of ordered NHs are generally between 300 and 600 nm/RIU in the visible range[33,43,98-100]. In regard to the other samples of the series under examination, corresponding to d_{NN} increasing from 110 to 178 nm, it was measured bulk sensitivity values associated with the transmittance minimum of (230±30)nm/RIU for NH(2min-1min), (296±32)nm/RIU for NH(1min-3min), (305±34) nm/RIU for NH(40s-5min) and (253±31) nm/RIU for NH(1min-2min).

4. Conclusions

In this study we have discussed the possibility of tuning the distribution properties of metal NH arrays by the optimization of the colloidal lithography deposition protocol usually applied under saturated adsorption conditions of the colloids. It has been demonstrated tunable NH-to-NH spacing and spatial correlation by discussing the influence of the presence of salt in the colloidal solution as well as the duration of the deposition step of both the polyelectrolyte adsorption layer and colloidal mask. In detail, we have presented short-range ordered NH distributions fabricated in optically thin (20 nm thick) gold films by colloidal lithography exploiting: i) a polydiallyldimethylammonium (PDDA) polyelectrolyte binding monolayer adsorbed for times ranging from 40 sec to 2 min, ii) salt-free solutions of polystyrene (80 nm-diameter) nanospheres, and iii) interplay of the deposition times to control the NH-to-NH spacing (d_{NN}, tuned from 110 to 178 nm). Unlike the conventional colloidal lithography protocol, we have considered a single polyelectrolyte layer rather than a polyelectrolyte multilayer and demonstrated a greatly simplified deposition protocol able to provide minimal agglomeration detrimental effects at the NH coverage suitable for sensing applications (NH diameter-to-periodicity of 0.5). The underlying working principle of our colloidal lithography deposition protocol is general, meaning that it can be applied to fabricate either optically thin and optically thick perforated metal films. Besides discussing the fabrication method, we have also investigated the properties of the samples by SEM analyses and statistical evaluation of coverage and NH-to-NH average distance to show their structural evolution depending on the deposition conditions. Such inspection has pointed out the key role of the balance between repulsive and attractive electrostatic forces in driving the degree of local ordering: decreasing NH-to-NH spacing above the agglomeration threshold can result in better correlated disorder under conditions leading to a d_{NN} closer

and closer to the NH-to-NH equilibrium spacing. Correlated disorder has been demonstrated for colloidal masks deposited under unsaturated adsorption condition from salt-free colloidal solutions by progressive increasing of the adsorption times. All of this allows obtaining characteristic transmission features (maxima and minima) in optical spectra as related to propagating and localized surface plasmon modes. It has been investigated and discussed transmittance, reflectance and absorbance spectra of the fabricated short range-ordered NH arrays. Furthermore, analogies between long- and short-range ordered systems have been demonstrated to hold under

deposition conditions ensuring an electrostatically correlated configuration with a characteristic average interparticle spacing. An important result of our combined analysis of the structural and optical properties of the deposited samples has been the identification of the average NH-to-NH spacing with a short-range periodicity of the NH distribution resulting from a method (the FFT analysis of the autocorrelation images) that is designed to disclose ordering length-scale rather than to perform statistical analysis. Also, we demonstrated a significant refractometric sensing (bulk sensitivity of ~309 nm/RIU) performances of our NH samples as compared to short range-ordered Au NH structures.

Conflicts of interest

There are no conflicts to declare.

Acknowledgements

This work was supported by a grant from the Ministry of Education, University and Research for the scientific program SIR2014Scientific Independence of young Researcher (RBSI1455LK). The authors acknowledge Adriano Colombelli (IMM-CNR, Lecce) for the acquisition of angle- and refractive index-dependent spectra, Enrico Melissano (IMM-CNR, Lecce) for the thermal deposition of gold films, Adriana Campa (IMM-CNR, Lecce) for preliminary SEM analyses, Antonio Pinna for technical support in SEM experiments and Maria Concetta Martucci (IMM-CNR, Lecce) for plasma treatments.

References

1 H.A. Bethe, *Phys. Rev*., 1944, **66,** 163.
2 T.W. Ebbesen, H.J. Lezec, H.F. Ghaemi, T. Thio and P.A. Wolff, *Nature*, 1998, **391**, 667.
3 C. Genet and T.W. Ebbesen, *Nature*, 2007, **445**, 39-46.
4 J. Henzie, J. Lee, M.H. Lee, W. Hasan and T.W. Odom, *Annu. Rev. Phys. Chem.,* 2009, **60**, 147–165.
5 F.J. Garcia-Vidal, L. Martin-Moreno, T.W. Ebbesen and L. Kuipers, *Reviews of Modern Physics*, 2010, **82(1)**, 729-787.
6 F.J. Garcia de Abajo, *Rev. Mod. Phys*., 2007, **79**, 1267.
7 H.F. Ghaemi, T. Thio, D.E. Grupp, T.W. Ebbesen and H.J. Lezec, Phys. Rev. B, 1998, 58, 6779-6782.
8 E.N. Economou, *Phys. Rev*., 1969, **182**, 539.
9 J.J. Burke, G.I. Stegeman and T. Tamir, *Phys. Rev. B*, 1986, **33**, 5186.
10 M. Sarrazin, J. P. Vigneron and J.-M. Vigoureux, *Phys. Rev. B*, 2003, **67**, 085415.
11 C. Genet, M.P. van Exter and J.P. Woerdman, *Opt. Commun*., 2003, **225**, 331.
12 S.-H. Chang, S.K. Gray and G.C. Schatz, *Opt. Express*, 2005, **13**, 3150.
13 D. Pacifici, H.J. Lezec, L.A. Sweatlock, R.J. Walters and H.A. Atwater, *Optics Express*, 2008, **16**, 9222.
14 T. Sannomiya, O. Scholder, K. Jefimovs, C. Hafner and A.B. Dahlin, *Small*, 2011, **7**, 1653.
15 L. Martín-Moreno, F.J. García-Vidal, H.J. Lezec, K.M. Pellerin, T. Thio, J.B. Pendry and T.W. Ebbesen, *Phys. Rev. Lett*., 2001, **86**, 1114.
16 H.J. Lezec and T. Thio, *Opt. Exp*., 2004, **12**, 3629.
17 H. Gao, J. Henzie, and T.W. Odom, *Nano Letters*, 2006, **6**, 2104.
18 S.-H. Chang, S.K. Gray and G.C. Schatz, *Opt. Express*, 2005, **13**, 3150.
19 M.M. Alkaisi, R.J. Blaikie, S.J. McNab, R. Cheung and D.R.S. Cumming, *Appl. Phys. Lett*., 1999, **75**, 3560.
20 X. Luo and T. Ishihara, *Opt Express*, 2004, **12**, 3055.
21 Y. Gong, A.G. Joly, P.Z. El-Khoury and W.P. Hess, *J. Phys. Chem. Lett*., 2014, **5**, 4243.
22 F.M. Huang, Y. Chen, F.J. Garcia de Abajo and N.I. Zheludev, *Appl. Phys. Lett*., 2007, **90**, 091119.
23 Y. Wang, N. Lu, W. Wang, L. Liu, L. Feng, Z. Zeng, H. Li, W. Xu, Z. Wu, W. Hu and L. Chi, *Nano Res.*, 2013, **6**, 159.
24 Y. Liu and S. Blair, *Opt. Lett*., 2003, **28**, 507.
25 S.H. Garrett, L.H. Smith and W.L. Barnes, *J. Mod. Opt*., 2005, **52**, 1105–1122.
26 A.G. Brolo, S.C. Kwok, M.G. Moffitt, R. Gordon, J. Riordon and K.L. Kavanagh, *J. Am. Chem. Soc*., 2005, **127**, 14936.
27 A.P. Blanchard-Dionne and M. Meunier, *Adv. Opt. Photon*., 2017, **9**, 891.
28 F. Yesilkoy, R.A. Terborg, J. Pello, A.A Belushkin, Y. Jahani, V. Pruneri and H. Altug, *Light: Science & Applications*, 2018, **7**, 17152.
29 R. Gordon, D. Sinton, K.L. Kavanagh and A.G. Brolo, *Acc. Chem. Res*., 2008, **41**, 1049.
30 A. Dahlin, M. Zäch, T. Rindzevicius, M. Käll, D.S. Sutherland and F. Höök, *J. Am. Chem. Soc.,* 2005, **127**, 5043.
31 T. Rindzevicius, Y. Alaverdyan, A.B. Dahlin, F. Höök, D.S. Sutherland and M. Käll, *Nano Lett*., 2005, **5**, 2335.
32 C. Escobedo, *Lab Chip*, 2013, **13**, 2445.
33 A. De Leebeeck, L.K.S. Kumar, V. de Lange, D. Sinton, R. Gordon and A.G. Brolo, *Analytical Chemistry*, 2007, **79**, 4094.
34 J. Ji, J.G. O'Connell, D.J.D. Carter and D.N. Larson, *Anal. Chem*., 2008, **80**, 2491.
35 A.B. Dahlin, *Analyst*, 2015, **140**, 4748.
36 M. Fana, G.F.S. Andrade and A.G. Brolo, *Analytica Chimica Acta*, 2011, **693**, 7.
37 E. Stewart, C.R. Anderton, L.B. Thompson, J. Maria, S.K. Gray, J.A. Rogers and R.G. Nuzzo, *Chem. Rev*., 2008, **108**, 494.
38 J Henzie, J. E. Barton, C.L. Stender and. T.W. Odom, *Acc. Chem. Res*., 2006, **39**, 249.
39 A.A. Yanik, M. Huang, A. Artar, T.Y. Chang and H. Altug, *Appl. Phys. Lett*., 2010, **96**, 021101.
40 E.-S. Kwak, J. Henzie, S.-H. Chang, S.K. Gray, G.C. Schatz and T.W. Odom, *Nano Lett.,* 2005, **5**, 1963.
41 M. Najiminaini, F. Vasefi, B. Kaminska and J.J.L. Carson, *Opt. Express*, 2011, **19**, 26186.
42 J.C. Sharpe, J.S. Mitchell, L. Lin, H. Sedoglavich and R.J. Blaikie, *Anal. Chem*., 2008, **80**, 2244.
43 A.G. Brolo, R. Gordon, B. Leathem and K.L. Kavanagh *Langmuir*, 2004, **20**, 4813.
44 D. Sinton, R. Gordon and A.G. Brolo, *Microfluid. Nanofluid*., 2008, **4**, 107.
45 F. Przybilla, C. Genet and T.W. Ebbesen, *Appl. Phys. Lett*., 2006, **89**, 121115.
46 F. Eftekhari, C. Escobedo, J. Ferreira, X. Duan, E.M. Girotto, A.G. Brolo, R. Gordon and D. Sinton, *Anal. Chem*., 2009, **81**, 4308.
47 V. Malyarchuk, F. Hua, N. Mack, V. Velasquez, J. White, R. Nuzzo and J. Rogers, *Opt. Exp*., 2005, **13**, 5669.
48 H. Im, S.H. Lee, N.J. Wittenberg, T.W. Johnson, N.C. Lindquist, P. Nagpal, D.J. Norris and S.-H. Oh, *ACS Nano*, 2011, **5**, 6244.
49 J. Henzie, M.H. Lee and T.W. Odom, *Nat. Nanotechnol*., 2007, **2**, 549.
50 E.-S. Kwak, J. Henzie, S.-H. Chang, S.K. Gray, G.C. Schatz and T.W. Odom, *Nano Lett*., 2005, **5**, 1963.
51 C.L. Haynes and R.P.J. Van Duyne, *Phys. Chem. B*, 2001, **105**, 5599.
52 M.-P. Murray-Methot, N. Menegazzo and J.-F. Masson, *Analyst*, 2008, **133**, 1714.

53 P. Hanarp, D.S. Sutherland, J. Gold and B. Kasemo, *Colloids and Surfaces A: Physicochem. Eng. Aspects*, 2003, **214**, 23.
54 J. Prikulis, P. Hanarp, L. Olofsson, D. Sutherland and M. Käll, *Nano Lett*., 2004, **4**, 1003.
55 S. Mei, T. Jie, L. Zhi-Yuan, C.G Bing-Ying, Z. Dao-Zhong, J. Ai-Zi and Y. Hai-Fang, *Chin. Phys. Lett*., 2006, **23**, 486.
56 M.Q. Liu, C.Y. Zhao, B.X. Wang and X. Fang, *Journal of the Optical Society of America B: Optical Physics*, 2018, **35**, 504.
57 F. Przybilla, C. Genet and T.W. Ebbesen, *Optics Express*, 2012, **20**, 4697.
58 T. Matsui, A. Agrawal, A. Nahata and Z. Valy Vardeny, *Nature*, 2007, **446**, 517.
59 T.H. Reilly, R.C. Tenent, T.M. Barnes, K.L. Rowlen and J. van de Lagemaat, *ACS Nano*, 2010, **4**, 615.
60 M.P. Jonsson, A.B. Dahlin, P. Jönsson and F. Höö, *Biointerphases*, 2008, **3**, FD30.
61 R. Kumar and S. Mujumdar, *Optics Communications*, 2016, **380**, 174.
62 S. Lee, D. Kim, S.-M. Kim, J.-A. Kim, T. Kim, D.-Y. Kima and M.-H. Yoon, *Nanoscale*, 2015, **7**, 14627.
63 R. A. McAloney, M. Sinyor, V. Dudnik and M. C. Goh, *Langmuir*, 2001, **17**, 6655.
64 N. M. Doskaliuk, P. M. Fochuk and Y. B. Khalavka, *Theoretical and Experimental Chemistry*, 2016, **52**, 85.
65 Y. M. Lvov, J.F. Rusling, D. L. Thomsen, F. Papadimitrakopoulos, T. Kawakamic and T. Kunitake, *Chem. Commun*., 1998, **0**, 1229.
66 S.G. Rodrigo, F.J. García-Vidal and L. Martín-Moreno, *Phys. Rev. Lett. B*, 2008, **77**, 075401.
67 Digital Micrograph software (DM Vers. 3.21.1374.0 http://www.gatan.com/).
68 N. Stéphant, B. Rondeau, J.-P. Gauthier, J. A. Cody and E. Fritsch, *Scanning*, 2014, **36**, 487.
69 R. Dhama, V. Caligiuri, L. Petti, A. R. Rashed, M. Rippa, R. Lento,; R. Termine, H. Caglayan, A. De Luca, *ACS Nano* 2018, **12**, 504.
70 V. Caligiuri, L. De Sio, L. Petti, R. Capasso, M. Rippa, M. G. Maglione, N. Tabiryan, C. Umeton, *Adv. Opt. Mater*. 2014, **2**, 950.
71 P. Hanarp, D.S. Sutherland, J. Gold, B. Kasemo, *Colloids and Surfaces A: Physicochem. Eng. Aspects* (2003), **214,** 23.
72 S. Syrenova, C. Wadell, C. Langhammer, *Nano Lett*. 2014, **14**, 2655.
73 C. Wadell, C. Langhammer, *Nanoscale* 2015, **7**, 10963.
74 J. J. Gray and R. T. Bonnecaze, *J. Chem. Phys*., 2001, **114**, 1366.
75 P.A. Kralchevsky and K. Nagayama, *Langmuir*, 1994, **10**, 23.
76 F. Burmeister, C. Schiifle, B. Keilhofer, C. Bechinger, J. Boneberg and P. Leiderer, *Chem. Eng. Technol*., 1998, **21**, 761.
77 D. Correia-Ledo, K.F. Gibson, A. Dhawan, M. Couture, T. Vo-Dinh, D. Graham and J.-F. Masson, *J. Phys. Chem. C*, 2012, **116**, 6884.
78 P. Zheng, S.K. Cushing, S. Suri and N. Wu, *Phys. Chem. Chem. Phys*., 2015, **17**, 21211.
79 R.A McAloney, M.C., Goh, *J. Phys. Chem. B* 1999, **103**, 10729.
80 I. Szilagyi, G. Trefalt, A. Tiraferri, P. Maroni, M. Borkovec, *Soft Matter*, 2014, **10**, 2479.
81 J. Bravo-Abad, A. Degiron, F. Przybilla, C. Genet, F.J. Garcia-Vidal, L. Martin-Moreno and T. W. Ebbesen, *Nature Physics*, 2006, **2**, 120.
82 W.A. Murray, S. Astilean and W.L. Barnes., *Phys. Rev. B*, 2004, **69**, 165407.
83 S. Spevak, A. Yu. Nikitin, E.V. Bezuglyi, A. Levchenko and A.V. Kats, *Phys. Rev. B*, 2009, **79**, 161406(R).
84 F. Yang, J.R. Sambles and G.W. Bradberry, *Phys. Rev. B*, 1991, **44**, 5855.
85 J. Braun, B. Gompf, T. Weiss, H. Giessen and M. Dressel, *Phys. Rev. B*, 2011, **84**, 155419.
View Article Online
DOI: 10.1039/C8NR09911A
86 S.G. Rodrigo, L. Martín-Moreno, A.Y. Nikitin, A.V. Kats,. S. Spevak and F.J. García-Vidal, *Optics Letters*, 2009, **34**, 4.
87 J. Parsons, E. Hendry, C.P. Burrows, B. Auguié, J.R. Sambles and W.L. Barnes, *Phys. Rev. B*, 2009, **79**, 073412.
88 J.H. Kim and P.J. Moyer, *Appl. Phys. Lett.*, 2006, **89**, 121106.
89 J. Braun, B. Gompf, G. Kobiela and M. Dressel, *Phys. Rev. Lett*., 2009, **103**, 203901.
90 S. Xiao, J. Zhang, L. Peng, C. Jeppesen, R. Malureanu, A. Kristensen and N. A. Mortensen, *Appl. Phys. Lett*., 2010, **97**, 071116.
91 T.-H. Park, N. Mirin, J. B. Lassiter, C.L. Nehl, N.J. Halas and P. Nordlander, *ACS Nano*, 2008, **2**, 25.
92 K. Xiong, G. Emilsson and A.B. Dahlin, *Analyst*, 2016, **141**, 3803.
93 S.H. Lee, N.C. Lindquist, N.J. Wittenberg, L.R. Jordan and S.-H. Oh, *Lab Chip*, 2012, **12**, 3882.
94 M. D Malinsky, K.L. Kelly, G.C. Schatz and R.P. Van Duyne, *J. Am. Chem. Soc.*, 2001, **123**, 1471.
95 T. Ohno, C. Wadell, S. Inagaki, J. Shi, Y. Nakamura, S. Matsushita and T. Sannomiya, *Opt. Mat. Express*, 2016, **6**, 1594.
96 V.E. Bochenkov, M. Frederiksen and D.S. Sutherland, *Optics Express*, 2013, **21**, 14763.
97 K. Cheng, S. Wang, Z. Cui, Q. Li, S. Dai and Z. Du, *Appl. Phys. Lett*., 2012, **100**, 253101.
98 C. Valsecchi and A.G. Brolo, *Langmuir*, 2013, **29**, 5638.
99 A. Lesuffleur, H. Im, N.C. Lindquist and S.H. Oh, *Appl. Phys. Lett*., 2007, **90**, 243110.
100 K.-L. Lee, W.-S. Wang and P.-K. Wei, *Plamonica*, 2008, **3**, 119.

Table of contents

View Article Online
DOI: 10.1039/C8NR09911A

Simplified colloidal lithography protocol (polyelectrolyte monolayer) for Au nanohole fabrication. Autocorrelation/FFT analysis of SEM images to disclose hidden short-range periodicities.